Proceedings of the Institute of Acoustics

4th International Conference on Synthetic Aperture Sonar and Synthetic Aperture Radar,
5-7 Septwember 2018, Lerici, Italy, Volume 40, pt. 2

ANALYSIS AND EXPLOITATION OF COMPLEX SAR PHENOMENA PRODUCED FROM VIBRATING TARGETS

B Corbett Centre for Electronic Warfare Information and Cyber, Cranfield University, Defence Academy of the United Kingdom, UK
D Andre Centre for Electronic Warfare Information and Cyber, Cranfield University, Defence Academy of the United Kingdom, UK
D Muff Centre for Intelligence Innovation (DSTL), RAF Wyton, UK
M Finnis Centre for Defence Engineering, Cranfield University, Defence Academy of the United Kingdom, UK
D Blacknell Centre for Intelligence Innovation (DSTL), RAF Wyton, UK

1 INTRODUCTION

Synthetic aperture radar (SAR) imagery has the potential to produce highly detailed images of a variety of landscapes and objects. However, SAR imagery can be affected by various physical phenomena, which can produce a range of artefacts within an image[1–3]. Understanding SAR phenomena is fundamental to advancing the SAR tools and analysis capabilities when identifying artefacts within SAR imagery.

One such artefact is a paired echo and is the result of a vibrating scatterer located within the imaging scene. From the authors previous work a running machine has been identified as a source for producing these phenomena within SAR imagery[3,4]. One challenging area where these phenomena are of particular interest is in the detection of running machinery within a building[3].

Through-wall SAR has recently experienced a large increase in research activity due to the wide range of applications in both defence and civilian sectors. Surface penetrating imagery using traditional SAR methods generates image products with varying degrees of accuracy and clarity[5]. However, a deeper understanding of the SAR phenomena applicable to through-wall radar imagery is required, leading to a clearer interpretation of the wave scattering processes in these challenging scenarios[4].

The purpose of this investigation is to focus on two types of phenomena and their interactions required to produce novel artefacts. The two SAR phenomena considered for investigation are (i) those produced from the effect of multipath and (ii) those produced from the imaging of a vibrating target[4].

Multipath will be considered because when two or more targets are within close proximity, *ghost* artefacts of the main target are produced down-range within the image. It has been hypothesised, if a target is near to a wall, it too will experience these multipath effects and therefore produce the same type of artefacts in the SAR image[4].

Target vibration is also being investigated because aspects of a running machine i.e. a generator, fan, etc. can be decomposed and considered as a point scattering target with a simple waveform motion, for example its position may be displaced in the form of a sinusoid wave[3,4].

Finally, this work aims to advance the art and capability in available SAR techniques which can be used to identify these artefacts within SAR imagery and extract valuable information about the sources of the artefacts[3,4].

2 SAR MULTIPATH PHENOMENA

Multipath is defined as; “The propagation of a wave from one point to another by more than one path”[6]. Hence, the wavefront of a transmitted electromagnetic wave will interact with multiple targets in the scene before being received by the antenna[1]. Multiple reflections of the wavefront can also

occur between targets. Each reflection the wave front experiences, increases the path length travelled by the wave from its transmit and receive locations. With SAR signal processing the result is repeated *ghosts* of the target being produced within the SAR image at predictable locations downrange for each target.

To simulate the multipath phenomena a point-to-point segmented ray approach for calculating the phase history for point targets within the desired scene is used[3,7,8].

In its simplest form the phase history can be calculated as follows,

$$\phi(n,m) = \exp\big(k(n)R(m)\big) \tag{1}$$

Where $k(n)$ is the complex wavenumber for the n^{th} frequency sample, of a transmitted electromagnetic (EM) pulse. $R(m)$ is the two-way ray range between the target and the EM source location, for the m^{th} measurement location.

We now consider the two shortest paths an EM ray can travel, starting from a single transmitter (source) location $\mathbf{A}$, then between two isotropic point scatterers ($\mathbf{T}_p, \mathbf{T}_l$) and then back to the source, as shown in Figure 1. Figure 1(a) shows a *4-ray-segment* path, i.e. the path taken by the ray is as follows; $\mathbf{A}(m) \rightarrow \mathbf{T}_p \rightarrow \mathbf{T}_l \rightarrow \mathbf{T}_p \rightarrow \mathbf{A}(m)$. Figure 1(b) shows a *3-ray-segment* path, i.e. the path taken by the ray is as follows; $\mathbf{A}(m) \rightarrow \mathbf{T}_p \rightarrow \mathbf{T}_l \rightarrow \mathbf{A}(m)$.

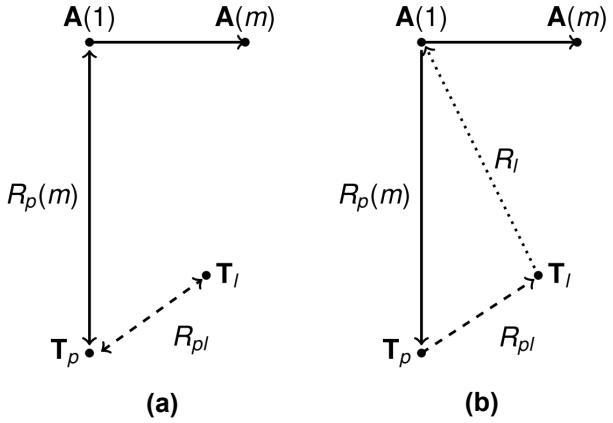

Figure 1: Generalised model of the ranges travelled by a transmitted EM wavefront from the antenna $\boldsymbol{A}(m)$, resulting in the formation of two types of multipath artefacts[7]:
(a) EM ray path one. The total path travelled by the EM ray is as follows, $T_p = 2R_p(m) + 2R_{pl}$.
(b) EM ray path two. The total path travelled by the EM ray is as follows, $T_p = R_p(m) + R_{pl} + R_l$.

Therefore, expanding the original phase history function from equation (1), with the inclusion of the new multipath range variables declared in Figure 1 (R_p, R_{pl}, R_l), yields equations (*2*) and (*3*), relating to the ray paths of Figure 1(a) and (b) respectively.

$$\phi_a(n,m) = \sum_{l=1}^{T}\sum_{o=1}^{M_b} \exp\big(k(n)\big[R_p(m) + oR_{pl[p\neq l]}\big]\big) \tag{2}$$

$$\phi_b(n,m) = \sum_{l=1}^{T} \exp\big(k(n)\big[R_p(m) + R_{pl[p\neq l]} + R_l(m)\big]\big) \tag{3}$$

Where T is the total number of targets in the scene. $R_p(m)$ is the two-way Euclidean distance between a single antenna position, $\mathbf{A}(m)$, and the first target of interaction in the scene $\mathbf{T}_p$. R_{pl} is the two-way Euclidean distance between the two targets within the scene, indicated by the subscript l. R_{pl} does not change with antenna position. M_b is the total number of multipath bounces induced

(represented by integer o) and is multiplied by R_{pl} to calculate the total distance travelled by a wavefront as it is reflected multiple times between two targets. Finally R_l is the one-way Euclidean distance back to the antenna ($\mathbf{A}(m)$) from the target $\mathbf{T}_l$.

Figure 2 shows three simulation images, formed using the backprojection[9] algorithm showing the different effects of multipath when different inter-scatterer distances are considered. Figure 2(a) and Figure 2(b) represent simulations of equations (2) and (3) respectively, whereas Figure 2(c) shows the result of the cumulative sum of equations (2) and (3); i.e. the generalised multipath SAR model.

Each simulation consists of two static targets, where; M_{pn} represents the n^{th} multipath bounce simulated. The parameters used in the simulations are as follows; Synthetic aperture: 2m (401 azimuthal samples), frequency range: 5-7GHz (1601 frequency samples). The simulation considers up to a maximum of 7 multipath bounces.

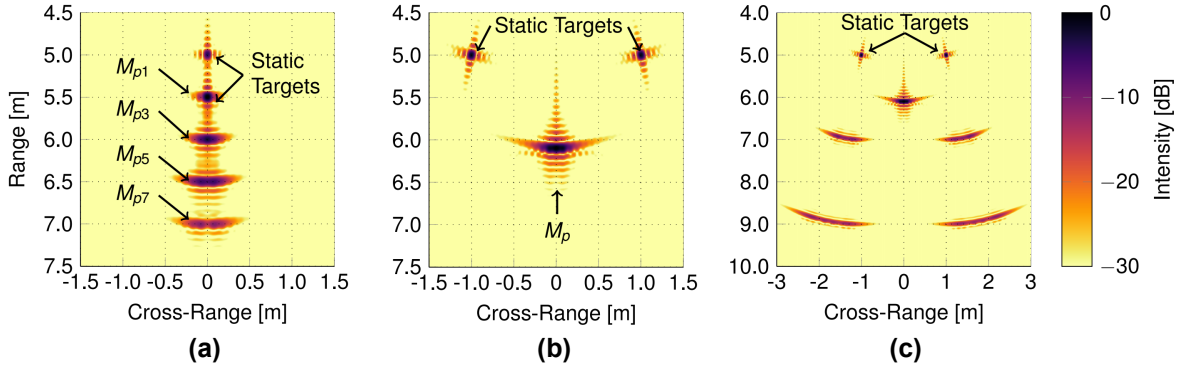

Figure 2: Simulation results produced from the developed SAR multipath numerical model. Two static targets are shown in each simulated scene. M_{pn} represents the n^{th} multipath bounce simulated.
(a) Multipath simulation of ray path one, shown in Figure 1(a)[4,7].
(b) Multipath simulation of ray path one, shown in Figure 1(b)[4,7].
(c) Multipath simulation of combined ray paths one and two[7].

3 SAR VIBRATION PHENOMENA

When using SAR signal processing to image a vibrating target, hence a target whose motion follows a repetitive waveform function, *fuzz-ball* artefacts are produced, comprising smeared signatures on the SAR image[2,7,10,11].

A detailed explanation to the physical principals that give rise to these paired-echo artefacts are presented in[2,4]. For example, a target vibrating with a sinusoidal displacement in the range dimension, the effect of its displacement can be expressed as a phase modulation term that is multiplied across the collected phase history[2,4]:

$$\phi(n,t) = \exp(ik(n)R(t))\exp(ik(n)\sin(2\pi f_v t)) \tag{4}$$

Where f_v is the vibration frequency and t is the respective time interval. The modulation term $\sin(2\pi f_v t_n)$ can be rewritten as two exponentials,

$$\sin(2\pi f_v t) = \frac{\exp(i2\pi f_v t) - \exp(-i2\pi f_v t)}{2i} \tag{5}$$

giving rise to two phase ramps where one is the complex conjugate of the other [2]. Hence, the signal response in the imaging space transforms from being a focused point into pairs of defocused artefacts on either side of the scatterer location in cross-range.

During the course of this work a novel asymmetric vibration artefact has been found. The artefact arises due to particular sawtooth target vibrations, which may occur in SAR images of partially occluded fans, say in air-conditioning units on roofs, where it is thought that these artefacts were first observed[4]. The novel asymmetric artefact could be simulated by simply replacing the exponential sinusoidal term from equation (4) with an exponential sawtooth waveform function, as follows[12].

$$\phi(n,t) = \exp(ik(n)R(t))\ \exp\left(ik(n)\left(A_v\frac{f_v}{t} - \left\lfloor\frac{f_v}{t}\right\rfloor\right)\right) \tag{6}$$

To validate the model for the novel phenomena experimental results are required. The controlled experimental setup used by the authors' in previous SAR vibrometry work has been reused here for validation[3, 7]. This is discussed in more detail in Sections 4.1 and 4.2.

Figure 3 compares several vibrating targets imaged using SAR signal processing, used to validate the developed numerical model for approximating the phase history of a vibrating target[7]. Figure 3(a) shows a simulated paired echo, produced from a vibrating point target whose motion follows a sinusoidal vibration waveform. Figure 3(b) and Figure **3**(c) show a direct comparison between a simulated and experimentally measured novel asymmetric artefact produced from a vibrating point target whose motion follows a sawtooth waveform.

The simulation and measurement parameters for all cases are kept consistent and are as follows: the scatterer's vibration amplitude was 14mm, with a 10Hz vibrational frequency given an antenna velocity of $2ms^{-1}$. The antennas traversed a 3m aperture (301 azimuthal samples) at a height of 2.81m. The radar transmitted over a 2GHz bandwidth from 4.5GHz to 6.5GHz in 801 pulses.

The results shown in Figure 3 shows a good likeness between the simulation and experimental data and hence justifies the use of these models in the authors further investigations.

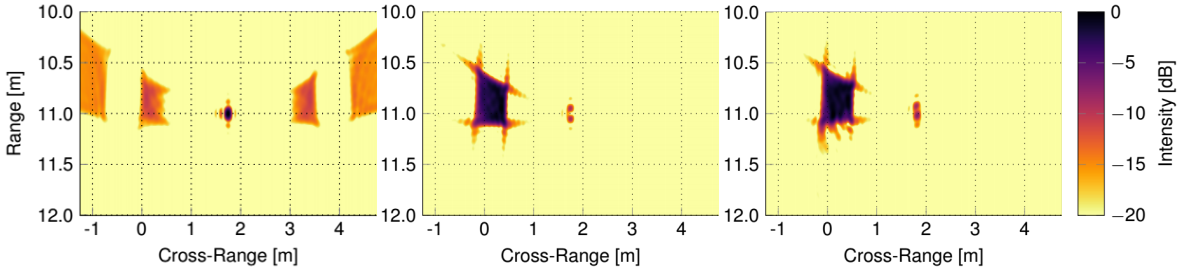

(a) **(b)** **(c)**

Figure 3: Simulated and experimental vibrating target results. Used to validate the developed numerical model for approximating the phase history of a vibrating target[7].
(a) Simulation of a vibrating target following a sinusoidal waveform, producing symmetrical echoes.
(b) Simulation of a vibrating target following a sawtooth waveform, producing asymmetrical echoes.
(c) Experimental validation of Figure 3(b).

4 COMBINATIONS OF SAR PHENOMENA

In real world scenarios, different SAR phenomena and their resultant image artefacts may not appear entirely on their own, but instead have the possibility to become coupled with each other. For example, if one considers a vibrating scatterer located in a scene in close proximity to other objects, it has been postulated by the authors that both multipath phenomena and vibration phenomena could become coupled to create a series of new artefacts visible within the SAR image.

To investigate this hypothesis, two test scenarios were considered, an initial test case and a through-wall scenario, representing the case of a generator located in close proximity to a wall, for example.

In order to validate the numerical results, measurements were taken using Cranfield University's Antennas and Ground-based SAR (AGBSAR) laboratory[13]. The radar system follows a stop/start approximation, i.e. the motion of the antennas pauses for each measurement. Therefore, one cannot have a continually moving target in the scene during the measurement process, hence a moving scatterer's motion needs to be synchronised to the radar system. The authors found a solution to this problem that has been validated in their previous work[3]. The synchronised moving target used is based on a Lego Mindstorms system which communicates wirelessly over Bluetooth to the AGBSAR radar system[3,4].

4.1 Initial Test Case

The experimental set-up and measurement results of this initial test case are shown in Figure 4. The geometry of the scene is configured so that the target under investigation is composed of two offset parallel metal plates.

The larger of the metal plates is static in the scene, oriented broadside to the radar, and is not directly visible to the radar system due to the radar absorbent material (RAM) attached along its antenna facing side, seen in Figure 4(a)[4]. The second, smaller plate, is part of a trihedral mounted on the moving Bluetooth Lego rover, and is orientated parallel to the larger plate. The trihedral is in the line-of-sight of the radar antenna, shown by the traced ray overlaid in Figure 4(a) which is shown to intercept with the target and return towards the direction of the antenna[4].

The measurement parameters used to for this initial test case are as follows: synthetic aperture: 2m (201 azimuthal samples), frequency range 4-8GHz (1601 frequency pulses), antenna height 1.8m, vibration amplitude: 10.71mm and a vibration frequency 10Hz given an effective antenna velocity of $2ms^{-1}$ [4].

The SAR measurement result is shown in Figure 4(b), which clearly shows the novel combined multipath and vibration artefacts, as described. Where M_{pn} represents the n^{th} number of multipath bounces; seven multipath bounce interactions are visible. Therefore this result validates the mechanism discussed as the origin of multipath-vibration artefacts.

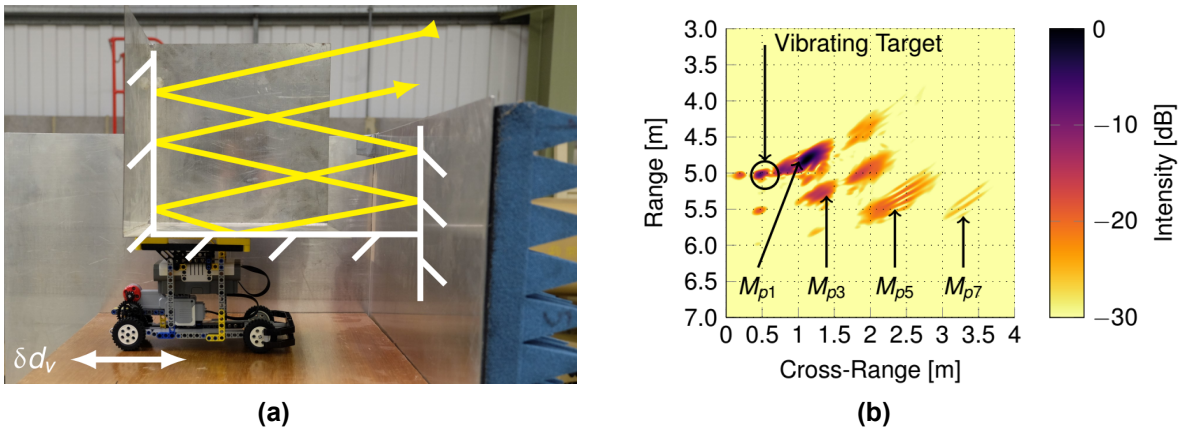

(a) **(b)**

Figure 4: Initial test measurement to produce combined multipath-vibration phenomena within a SAR image[4,7].
(a) Experimental set-up used to create multipath-vibration phenomena.
(b) Initial test case measurement result showing the novel multipath-vibration phenomena described. Where M_{pn} represents the n^{th} number of multipath bounces.

4.2 Through-Wall Measurement

Building upon the initial test case the authors proceeded to implement a through-wall measurement with the aim of creating a more realistic scenario. The vibrating target now replicates a generator located in situ next to a masonry wall.

The experimental set-up for this through-wall measurement is shown in Figure 5(a). Here the first scatterer, i.e. the metal plate closest to the radar antenna in the measurement set-up of Figure 4, has been replaced with a dielectric medium: a concrete masonry block wall. The wall itself is loosely built and the blocks are not secured in place by mortar/cement. The wall intercepts all lines-of-sight between the antenna and the target and is located approximately 4m downrange of the antenna.

The SAR measurement was undertaken using the following parameters: synthetic aperture: 1.25m (125 azimuthal samples), frequency range: 2-5GHz (1601 frequency pulses), antenna height 0.86m, vibration amplitude: 21.43mm and a vibration frequency 10Hz given an effective antenna velocity of $2\mathrm{ms}^{-1}$.

The resultant SAR image of this measurement is shown in Figure 5(b). The wall is clearly visible and five multipath bounce interactions have been identified within the image. Due to the attenuation effects of the dielectric concrete wall the artefacts now have a lower intensity and therefore this results in fewer multipath-vibration artefacts being visible within the given dynamic range, when compared with Figure 4(b).

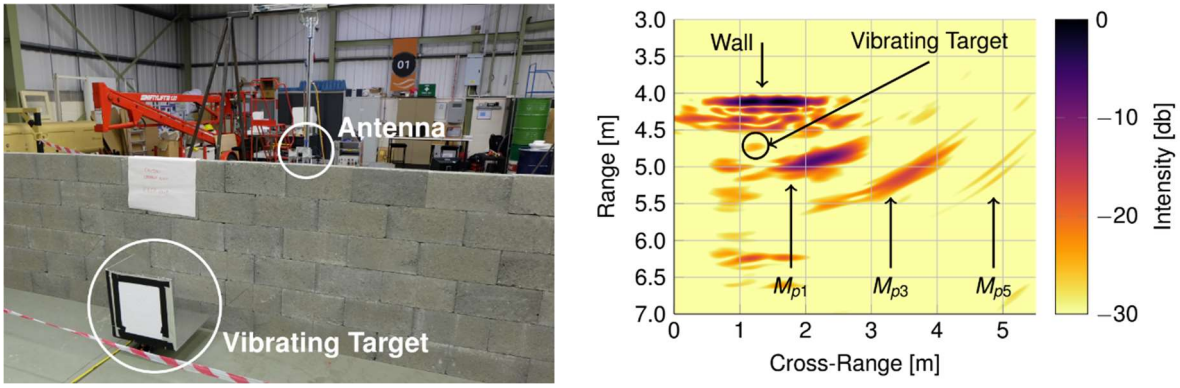

(a) **(b)**

Figure 5: Through-wall measurement to see if combined multipath-vibration phenomena can occur from this scenario[4,7].

(a) Experimental set-up used for through-wall measurements.

(b) Measurement result of through-wall induced multipath-vibration artefacts. Where M_{pn} represents the n^{th} number of multipath bounces.

5 EXPLOITING SAR PHENOMENA FOR INTELLIGENCE ANALYSIS

Usually when one is confronted with a SAR image containing vibration target phenomenology the consensus is to either remove it or focus it. There has been considerable work accomplished in these two areas, producing a variety of suppression and focusing techniques[14–16]. However, little has been done towards understanding the unfocused artefacts and how they can be exploited from the image to aid in the data analysis process[8,17].

It is important to find practical applications of both theoretical and experimental work. Hence, the aim of this piece of work is to take the authors novel understanding of vibration artefact localisation[8,17] and provide tools for exploitation within a practical piece of analyst aid software.

The purpose of the program would be simple; aid in the SAR image analysis process to allow the user to make a detailed estimation of the vibration parameters for a suspected vibrating target within a given SAR image[17]. This would be accomplished through the use of a simple graphical user interface (GUI), where one would identify suspect artefacts and then based on their visual geometry make an estimation about the target's vibration parameters[8,17].

5.1 ANALYST AID SOFTWARE

The GUI interface of the analyst aid software is shown in Figure 6. It works by creating a superimposed output from the authors vibration model[8] at a desired coordinate location[17]. Once the superimposed plot and the vibration artefact line-up, an estimation to the vibration of the target can be made[17].

Figure 6(a) shows the software tested on a simulated SAR image. The simulated scene contains a randomly generated group of static and vibrating isotropic point scatterers in the SAR-near-field, between 8-12m down-range of the antennas. There are thirty scatterers in total, four of which are vibrating with the same 10Hz frequency, and a 5mm amplitude. The parameters used to generate this data set are as follows; the antennas traversed a 2m aperture at a velocity of $2\mathrm{ms}^{-1}$, with an elevation height of 0m. The simulated radar, transmitted 1601 frequency samples over a 2GHz bandwidth from 9GHz to 11GHz.

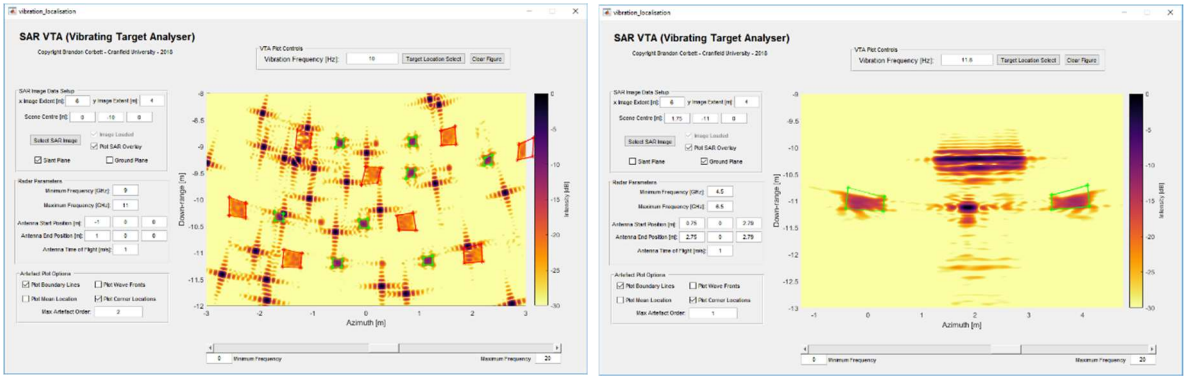

(a) **(b)**

Figure 6: Synthetic Aperture Radar Vibrating Target Analyser (SAR VTA) program[17]. SAR artefacts are clearly visible in both images and their perimeter has been highlighted by the program.
(a) SAR VTA used with a simulated test data set showing a random placement of thirty point scatterers, four of which are vibrating[17].
(b) SAR VTA used on the authors previous experimental through-wall SAR data set of a vibrating target[3].

In Figure 6(b) the authors tested the software on their previously collected through-wall measurement data set of a vibrating target[3], to represent a realistic case study of where the software could be used. Figure 6 results reveal how influential this type software could be when analysing SAR imagery. The software has allowed the user to precisely pinpoint suspect targets and then make an estimation of the vibrational frequency.

6 CONCLUSION

A variety of novel vibrating scatterer related SAR phenomena have been predicted through numerical SAR simulation and have been imaged in the laboratory.

The computations demonstrated that the edges of a dielectric medium can act as a source for multipath effects, leading to the hypothesis that SAR artefacts can arise from through-wall SAR

imagery. This mechanism was validated through several experimental measurements, undertaken at Cranfield University's Antennas and Ground-based SAR laboratory, yielding results that closely match those predicted.

Work towards exploiting this new understanding has begun in an attempt to apply this knowledge to real through-wall intelligence applications. This is being done through a user orientated approach to developing the software tools required to aid the user in identifying vibration artefacts measured in SAR imagery.

7 REFERENCES

1 D. Andre, R. D. Hill, and C. P. Moate, “Multipath Simulation And Removal from SAR Imagery,” in *Algorithms for Synthetic Aperture Radar Imagery*, 2008.

2 D. Andre, D. Blacknell, D. Muff, and M. Nottingham, “The physics of vibrating scatterers in SAR imagery,” in *Algorithms for Synthetic Aperture Radar Imagery XVIII*, 2011.

3 B. Corbett, D. Andre, and M. Finnis, “Through-Wall Detection and Imaging of a Vibrating Target Using Synthetic Aperture Radar,” in *IET Electronics Letters*, 2017, vol. 53, no. 15, pp. 991–995.

4 B. Corbett, D. Andre, D. Muff, I. Morrow, and M. Finnis, “Imaging SAR Phenomenology of Concealed Vibrating Targets,” in *12th European Conference on Synthetic Aperture Radar EUSAR.*, 2018, pp. 1–5.

5 M. G. Amin and F. Ahmad, “Through-the-Wall Radar Imaging: Theory and Applications,” in *Academic Press Library in Signal Processing*, 1st ed., vol. 2, N. D. Sidiropoulos, F. Gini, and R. Chellappa, Eds. Elsevier, 2014, pp. 857–909.

6 R. J. Sullivan, *Microwave Radar : Imaging and Advanced Concepts*. Norwood, MA: Artech House, INC, 2000.

7 B. Corbett, D. Andre, D. Muff, and M. Finnis, “Understanding Complex Synthetic Aperture Radar Phenomenology of Concealed Vibrating Targets,” *To Be Publ.*, 2018.

8 B. Corbett, D. Andre, and M. Finnis, “Localising Unfocused Vibrating Phenomena In Near-Field Synthetic Aperture Radar Imagery,” *To Be Publ.*, 2018.

9 D. C. Munson, J. D. O’brien, and W. Kenneth Jenkins, “A Tomographic Formulation of Spotlight-Mode Synthetic Aperture Radar,” *Proc. IEEE*, vol. 71, no. 8, pp. 917–925, 1983.

10 W. G. Carrara, R. S. Goodman, and R. M. Majewski, *Spotlight Synthetic Aperture Radar, Signal Processing Algorithms*, First. Artech House, INC, 1995.

11 M. Ruegg, E. Meier, and D. Nuesch, “Constant Motion, Acceleration, Vibration, and Rotation of Objects in SAR Data,” in *SAR Image Analysis, Modeling, and Techniques VII*, 2005, vol. 5980, pp. 598005-598005–12.

12 E. W. Weisstein, “Square Wave,” *Mathworld-A Wolfram Web Resource*, 2017. [Online]. Available: http://mathworld.wolfram.com/ SquareWave.html.

13 D. Andre, K. Morrison, D. Blacknell, D. Muff, M. Nottingham, and C. Stevenson, “Very High Resolution Coherent Change Detection,” *Radar Conf. (RadarCon), 2015 IEEE*, pp. 634–639, 2015.

14 Y. Zhang, J. Sun, P. Lei, and W. Hong, “SAR-based Paired Echo Focusing and Suppression of Vibrating Targets,” *IEEE Trans. Geosci. Remote Sens.*, vol. 52, no. 12, pp. 7593–7605, 2014.

15 W. Zhang, C. Tong, Q. Zhang, Y. Zhang, and X. Zhang, “Extraction of Vibrating Features with Dual-Channel Fixed-Receiver Bistatic SAR,” *IEEE Geosci. Remote Sens. Lett.*, vol. 9, no. 3, pp. 507–511, 2012.

16 Q. Wang, M. Pepin, A. Wright, R. Dunkel, T. Atwood, B. Santhanam, W. Gerstle, A. W. Doerry, and M. M. Hayat, “Reduction of Vibration-Induced Artifacts in Synthetic Aperture Radar Imagery,” *IEEE Trans. Geosci. Remote Sens.*, vol. 52, no. 6, pp. 3063–3073, 2014.

17 B. Corbett, D. Andre, and M. Finnis, “Software Exploitation Ability To Localise Unfocused Vibrating Scatterer Phenomena in Synthetic Aperture Radar Imagery,” *To Be Publ.*, 2018.